MEASUREMENTS OF SHEAR-WAVE AZIMUTHAL ANISOTROPY WITH CROSS-DIPOLE LOGS

Guo Tao, Arthur C.H. Cheng, and M.N.Toksöz

Earth Resources Laboratory
Department of Earth, Atmospheric, and Planetary Sciences
Massachusetts Institute of Technology
Cambridge, MA 02139

ABSTRACT

Three methods for analyzing azimuthal anisotropy from cross-dipole logs are applied to data from the Powder River Basin in Wyoming. These techniques are based on the phenomena of flexural wave splitting in anisotropic materials and are analogous to the techniques used for VSP data processing. The four-component cross-dipole logging data obtained with a Schumberger tool from a vertically-fractured section of 56 m at a depth of 3550 m are processed with three different techniques. The results demonstrate that the non-orthogonal rotation method works best for the data. The results from the linear transform and polar energy spectrum methods are acceptable. The linear transform processing takes much less computing time, while the polar energy spectrum method is computationally-intensive.

INTRODUCTION

Laboratory and field observations have demonstrated that, if a formation exhibits shear-wave anisotropy, i.e., there is a directional crack system or ambient stress field, the flexural mode will propagate anisotropically with respect to their polarization direction. Intuitively, one might expect that a flexural mode polarized along the fast or slow direction will propagate at zero frequency with fast or slow formation shear velocities, respectively. This phenomenon could be used to characterize the formation anisotropy in principle.

A simple mode calculation made by Leveille and Seriff (1989) proved that this is most likely the case. Further calculations carried out by Ellefsen (1990) and Cheng (1994) show that in the presence of azimuthal anisotropy, two (quasi-) flexural modes exist—a slow flexural wave for which the particle displacements are aligned with the

polarization of the slow shear wave, and a fast flexural wave for which the particle displacements are aligned with the polarization of the fast shear wave. Sinha (1991) also calculated the flexural mode excitation amplitudes in the presence of transverse isotropy.

Ellefsen (1990) showed that for normal modes propagating along a borehole that is parallel to the symmetry axis of a transversely isotropic earth model, the shapes of the phase and group velocity curves are like those for an isotropic model. The phase velocities of these modes do not exceed the phase velocities of the two S-waves propagating parallel to the symmetry axis. Furthermore, the characteristics of the displacements and pressures are identical to those for an isotropic mode. The orientations of the two flexural waves and the two screw waves are arbitrary, just as the polarizations of the two S-waves propagating parallel to the symmetry axis are arbitrary. For the case of an orthorhombic model with an intersection of two symmetry planes being parallel to borehole, the phase and group velocities do not exceed the phase velocity of the slow qS-wave whose wavenumber vector is parallel to the borehole. The two quasi-flexural waves have different phase and group velocities, and the differences are large at low frequencies but small at high frequencies.

Using the perturbation model, Sinha (1991) calculated the flexural wave propagation characteristics in a liquid-filled borehole in an anisotropic formation. His results for a slow formation (Austin chalk) that exhibits the symmetry of a TI medium confirmed that the low-frequency asymptote of the flexural wave velocity merges with the quasi-S wave velocity for the selected propagation direction and the flexure direction parallel to the shear polarization directions. The high frequency asymptote of the flexural wave velocity turns out to be the Scholte wave velocity appropriate for the propagation and polarization directions. However, his results demonstrated that the difference in phase velocity between the two orthogonally polarized quasi-flexural waves is essentially independent of frequency under this condition. This phase velocity difference is a maximum when the TI symmetry axis inclines 90^o with respect to the direction of wave propagation, and diminishes when the inclining angle becomes less than 45^o. The frequency dependence of the amplitude difference for the two orthogonally polarized quasi-flexural waves is significant in this case. The synthetic waveforms he calculated for dipole sources directed along the S_H- and S_V-wave polarization directions show that, the early arrivals are dominated by the less dispersive, low-frequency components. His models also show that waveform amplitudes are significantly larger for the fast flexural wave than for the slow flexural wave for the same source amplitudes. Finally, the dispersive features of the flexural arrivals are shown to be quite similar to those calculated for the case of a liquid-filled borehole of the same radius surrounded by an isotropic, slow formation.

Hatchell and Cowles (1992) described a spectral method for determining the magnitude and direction of shear wave anisotropy in a weakly anisotropic ($\Delta V_s/V_s \ll 1$) formation, using full waveform dipole logging data. Esmersoy *et al.* (1994) employed the technique of data matrix rotation, which resembles a method for VSP data processing, to measure the sonic-scale shear anisotropy of a formation with dipole logging

data. However, the flexural mode and borehole logging environment are very different from the VSP application. The dispersion of the flexural mode leads to a frequency dependence in amplitude which could mix with the effects attributed to anisotropy and lead to possible errors in interpretation. Further studies are necessary to identify the conditions under which VSP methods can be applied to dipole logging data processing.

In this paper, we examine three methods for determining the anisotropy parameters with a cross-dipole data set from ARCO's Red Mountain Well in the Powder River Basin in Wyoming. The data are from a depth interval of 56 m (185 ft) that was proved by other independent information (FMI/FMS) to be full of vertical fractures and therefore expected to demonstrate transversely isotropic (TI) properties.

BRIEF DESCRIPTION OF THE THREE METHODS FOR DETERMINING SHEAR-WAVE ANISOTROPY IN VSP SURVEYS

Definition of Anisotropy Parameters and Basic Assumption

Acquisition Geometry

Figure 1 shows a schematic diagram of a fluid-filled borehole of radius a. The surrounding formation exhibits the symmetry of a TI medium whose symmetry axis (Z) is normal to the borehole axis (Z'). This is analogous to the anisotropy in the earth caused by stress-aligned, fluid-filled inclusions uniformly distributed between the transmitter and receivers.

Figure 2 shows the coordinate system with the origin at the transmitter or receiver plane. We assume that there is no angular misalignment between the transmitter and receiver section of the tool. Two orthogonal dipole transmitters, designated T_1 and T_2, are located at the same depth and on the axis of a vertical circular borehole. Two orthogonal dipole receivers, $R1$ and $R2$, are located on the axis of the borehole a distance L away from the transmitters. In the case of an array of receiver pairs, the distance between transmitters and each receiver pair is designated as L_1, L_2, etc. The angle between the fast and slow shear wave polarization directions and the dipole T_1 on this plane is designated as θ_1 and θ_2, respectively.

The basic assumptions behind these VSP methods for anisotropy measurements are as follows:

1. *Homogeneous anisotropy.* The polarizations of quasi-shear waves do not change with depth within the medium between source and receiver sets.

2. *Polarizations of the split shear waves.* The polarizations of split flexural waves are fixed for a given raypath direction. This implies that the angles θ_1 and θ_2 are invariant over a time window that covers a specific shear wave arrival.

3. *Principle of superposition.* It is always assumed that a source vector F with response polarization function $F(\omega, t)$ can be decomposed into two components,

F_1 andF_2, along the P_1 and P_2 directions with response functions $F_1(\omega, t)$ and $F_2(\omega, t)$, respectively. The wavefield excited by source vector F in the medium is equivalent to the wavefield excited simultaneously by F_1 andF_2.

Basic Relationship

With the above assumptions, the following essential equations can be formulated:

$$\begin{aligned} F_1(\omega, t) &= -F(\omega, t) cos\theta_2 / sin(\theta_2 - \theta_1) \\ F_2(\omega, t) &= F(\omega, t) cos\theta_1 / sin(\theta_2 - \theta_1). \end{aligned} \tag{1}$$

Two principal time series $qs_1(t)$ and $qs_2(t)$ are then defined to facilitate and quantify the anisotropy measurements. The $qs_1(t)$ is referred to as the fast split shear wave and is defined as the time series which results when the receiver and a source vector F are both polarized along p_1. Similarly, the $qS_2(t)$ is the slow split shear wave which is the time series generated when the receiver and a source vector F are both polarized along p_2. Two transformed time series $V_1(t)$ and $V_2(t)$ are introduced as the sum and difference, respectively, of the principal time series $qs_1(t)$ and $qs_2(t)$:

$$\begin{aligned} V_1(t) &= qs_1(t) + qs_2(t) \\ V_2(t) &= qs_1(t) - qs_2(t). \end{aligned} \tag{2}$$

According to the principle of superposition as shown Figure 2, the T_1-source (X-direction)can be decomposed into two components. The amplitudes of the fast and slower split shear waves excited by T_1 can thus be expressed as:

$$\begin{aligned} & qs_1(t) sin(\theta_2) / sin(\theta_2 - \theta_1) \\ & -qs_2(t) sin(\theta_1) / sin(\theta_2 - \theta_1). \end{aligned} \tag{3}$$

respectively. Similarly, the amplitudes of the fast and slower shear waves excited by the T_2 are:

$$\begin{aligned} & -qs_1(t) cos(\theta_2) / sin(\theta_2 - \theta_1) \\ & qs_2(t) cos(\theta_1) / sin(\theta_2 - \theta_1). \end{aligned} \tag{4}$$

Now the four component time series $s_{ij}(t)$ recorded from T_1 and T_2 -sources ($j = 1, 2$) at R_1 and R_2 receivers ($i = 1, 2$) can be written as:

$$\begin{aligned} s_{11}(t) &= [qs_1(t) sin(\theta_2) cos(\theta_1) - qs_2(t) sin(\theta_1) cos(\theta_2)] / sin(\theta_2 - \theta_1) \\ s_{21}(t) &= [qs_1(t) sin(\theta_2) sin(\theta_1) - qs_2(t) sin(\theta_1) sin(\theta_2)] / sin(\theta_2 - \theta_1) \\ s_{12}(t) &= [-qs_1(t) cos(\theta_2) cos(\theta_1) + qs_2(t) cos(\theta_1) cos(\theta_2)] / sin(\theta_2 - \theta_1) \\ s_{22}(t) &= [-qs_1(t) sin(\theta_1) cos(\theta_2) + qs_2(t) sin(\theta_2) cos(\theta_1)] / sin(\theta_2 - \theta_1). \end{aligned} \tag{5}$$

These are basic relations between the recorded components and the principal time series of split shear waves. For the case of flexural waves, the same relations could be derived if the basic assumptions are also applicable to dipole logging. This is an important point when techniques originally used in VSP data processing are to be extended to dipole logging data processing.

Three Methods for Determining Principal Time Series and Anisotropy Directions

We need to determine $qs_1(t)$ and $qs_2(t)$ and θ_1 and θ_2 from the recorded time series $s_{ij}(t)$ in order to determine the anisotropy parameters. There are three time domain methods developed primarily for VSP data processing which are available. The rotation scanning technique first developed by Alford (1986) and Thomsen (1988) and refined for dipole logging data processing by Nolte and Cheng (1996); the linear-transform technique developed by Li and Crampin (1993); and the polar energy spectrum method to determine anisotropy directions, proposed by Igel and Crampin (1990). These techniques will be analyzed and examined with the data from dipole logging in a TI formation.

Rotation Scanning Technique

Assuming the two split flexural waves are orthogonally polarized, let $\theta_1 = \theta_2 - \pi/2 = \theta$, and combining the equations 2 to 5, the solution for the principal time series is straightforward:

$$\begin{aligned} qs_1(t) &= cos^2(\theta)s_{11}(t) + sin(\theta)cos(\theta)[s_{21}(t) + s_{12}(t)] + sin^2(\theta)s_{22}(t) \\ qs_2(t) &= sin^2(\theta)s_{11}(t) - sin(\theta)cos(\theta)[s_{21}(t) + s_{12}(t)] + cos^2(\theta)s_{22}(t) \end{aligned} \tag{6}$$

and

$$\begin{aligned} 0 &= sin^2(\theta)s_{21}(t) + sin(\theta)cos(\theta)[s_{11}(t) - s_{22}(t)] - cos^2(\theta)s_{12}(t) \\ 0 &= sin^2(\theta)s_{12}(t) + sin(\theta)cos(\theta)[s_{11}(t) - s_{22}(t)] - cos^2(\theta)s_{21}(t). \end{aligned} \tag{7}$$

Equations 6 and 7 can be calculated for a sequence of values of θ, the value chosen for the final θ is that for which the linear combination of data on the right-hand side of equation 7 is approximately zero at all times for the whole traces. This angle is then used in equation 6 to determine the principal time series. Nolte and Cheng (1996) present a method that is able to handle the case of non-orthogonally polarized waves and, moreover, is computationally more efficient than Alford's technique. Their method is based on the eigenvalue decomposition of an asymmetric matrix and a least-squares minimization of its off-diagonal components. In the case of orthogonally polarized waves their method will yield exactly the same results as Alford rotation. In this study, the results of applying the method of Nolte and Cheng (1996) are employed for comparison.

Linear Transform Technique

Li and Crampin (1993) introduced a set of linear transforms to the four component data sets:

$$\begin{aligned} D_1(t) &= s_{11}(t) - s_{22}(t) \\ D_2(t) &= s_{21}(t) + s_{12}(t) \\ D_3(t) &= s_{11}(t) + s_{22}(t) \\ D_4(t) &= s_{12}(t) - s_{21}(t). \end{aligned} \tag{8}$$

Combining this equation with equations 2 to 5, we have:

$$\begin{aligned} D_1(t) &= [qs_1(t) - qs_2(t)]sin(\theta_2 + \theta_1)/sin(\theta_2 - \theta_1) \\ D_2(t) &= [qs_2(t) - qs_1(t)]cos(\theta_2 + \theta_1)/sin(\theta_2 - \theta_1) \\ D_3(t) &= qs_1(t) + qs_2(t) \\ D_4(t) &= [qs_1(t) - qs_2(t)]cos(\theta_2 - \theta_1)/sin(\theta_2 - \theta_1). \end{aligned} \tag{9}$$

By introducing another time series,

$$U(t) = [qs_1(t) - qs_2(t)]/sin(\theta_2 - \theta_1) \tag{10}$$

then equations 9 can be written:

$$\begin{aligned} D_1(t) &= U(t)sin(\theta_2 + \theta_1) \\ D_2(t) &= -U(t)cos(\theta_2 + \theta_1) \\ D_3(t) &= U(t)sin(\theta_2 - \theta_1) \\ D_4(t) &= -U(t)cos(\theta_2 - \theta_1). \end{aligned} \tag{11}$$

This equation shows that $U(t)$ is linear motion in coordinate system $(D1, -D2)$ and $(D3, -D4)$, with angle $\theta_2 + \theta_1$ to the $D1$ axis and $\theta_2 - \theta_1$ to the $D3$ axis, respectively. Therefore, we can uniquely determine $U(t)$, θ_2, and θ_1. Consequently, $V_1(t) = qs_1(t) + qs_2(t)$ and $V_2(t) = qs_1(t) - qs_2(t)$ can be calculated from the four component records s_{ij}. In practice, this is achieved by first estimating the covariance matrix of $D_1(t)$ to $-D_2(t)$ and $D_3(t)$ to $-D_4(t)$, then $\theta_2 + \theta_1$ and $\theta_2 - \theta_1$ can be calculated. Finally, the two principal time series are calculated using equation 2.

Polar Energy Spectrum

Igel and Crampin (1990) introduced a technique for identifying shear wave polarizations when the data has been recorded with more than one source orientation. This technique yields direct information about the shear wave splitting and allows the polarizations of the split shear waves to be recognized in the presence of interference which leads to elliptical particle motion. This method, which is analogous to optical experiments, measures

the polar energy as a function of polarization after propagation through formations. For a given source polarization θ, two fixed orthogonal directions are taken in the medium with components of the recorded displacement vector, $x(\theta,t)$ and $y(\theta,t)$, measured in the coordinate system in Figure 3. Let $x_1(t)$, $y_1(t)$ and $x_2(t)$, $y_2(t)$ be the displacements for the two source orientations θ_1 and θ_2, respectively. When $\theta_1 - \theta_2 = 90^o$, as in the case of dipole logging, the displacements become:

$$\begin{aligned} x(\theta,t) &= cos(\theta-\theta_1)x_1(t) + sin(\theta-\theta_1)x_2(t) \\ y(\theta,t) &= cos(\theta-\theta_1)y_1(t) + sin(\theta-\theta_1)y_2(t) \end{aligned} \tag{12}$$

The instantaneous direction of the displacement vector in the horizontal plane is

$$\phi(\theta,t) = tan^{-1}(y(\theta,t)/x(\theta,t)) \tag{13}$$

where both $\phi(\theta,t)$ and θ are specified between 0^o and 180^o. For a given source orientation θ, seismic energy is sorted in the time interval $t_2 - t_1$ as a function of displacement direction ϕ between 0^0 and 180^o

$$F(\theta,\phi) = \sum_{t_1}^{t_2} E(t,\phi_k,\theta) \tag{14}$$

where $E(t,\phi_k,\theta)$ is the seismogram energy at time t for direction ϕ in the interval $\phi_k - \Delta\phi \leq \phi_k + \Delta\phi$ for source orientation θ. $F(\theta,\phi)$ is calculated for $0^0 \leq \theta \leq 180^o$ in 1^o steps, representing the full range of possible source orientations. $F(\theta,\phi)$ ranges over a square array of bins, where the elements correspond to relative total energy associated with polarization direction ϕ as a function of source polarization. Sums of energy, E, for each displacement direction ϕ for all calculated source orientations θ, are determined, and the directions of the two maximum values of E are selected as the two principal directions.

$$E(\phi) = \sum_{\theta=0^o}^{180^o} F(\phi,\theta). \tag{15}$$

Summary

Three methods for analyzing azimuthal anisotropy from VSP data are described. These techniques are applied to dipole logging data processing, based on the similarity between phenomena of shear wave and flexural wave splitting in anisotropic materials. All these methods use four component measurements. The linear-transform technique needs less computation and can handle the case of non-orthogonal splitting of shear waves, if there are two orthogonally polarized transmitters and receivers available and their alignments are perfect. The requirement for the alignment of source and receiver could be relaxed

if the fast and slower flexural modes are orthogonally polarized. The rotating data matrix technique is computationally intensive. The development of Nolte and Cheng improved this rotation technique in both computational efficiency and applicability to non-orthogonal splitting cases. The polar energy spectrum method may be robust in picking up polarization direction and hence the directions of principal anisotropy axes. It is also computationally intensive.

CROSS-DIPOLE LOGGING DATA USED IN THIS STUDY

Figures 4 and 5 show a section [15.24 m (50 ft) from depth 3521 m to 3536 m] of the cross-dipole waveform from one cross-line and one in-line measurement of receiver number five and the upper source. Figure 6 shows the logging tool azimuthal orientation recorded for the same section, and the variation of travel times of the first (solid line) and second (dashed line) dipole in-line measurements at equal-offset receivers. These times are obtained by picking an early zero crossing in the waveforms. Because the tool orientation changes by about 180 degrees in this section, the cross-component amplitudes go through minima at around 3529 m and 3534 mm, and the waveforms change sign on either side of these minima. This is consistent with an azimuthal anisotropic model. The data set used in this study is from a section of about 56 m (185 ft) in depth, and consisting of four components at seven-receiver positions. The data from receiver number four is not usable, probably due to instrument problems.

RESULTS OF APPLYING PROCESSING TECHNIQUES TO THE DATA SET

To compare the three techniques, we first apply them to a small portion of the data set. Afterwards, the results from processing the whole data set are examined. Figure 7 shows an 8 m section of the cross-component waveforms in a time window from 1.5 ms to 4 ms. The two minima can be seen more clearly along with the waveform change on either side of these minima. Figure 8 shows the four component waveforms at receiver five for shot number 165 taken from the smaller section in Figure 7.

As discussed by Nolte and Cheng (1996), the Schlumberger dipole tool has two sources which are spaced 0.152 m (0.5 ft) apart from each other. As a result, when data are collected with this tool the components for the x-source are not exactly aligned with those of the y-source since the tool has moved by 0.152 m in depth between the source firings. This movement is usually accompanied by a rotation by some angle γ. In this study, before we determine the polarizations we always correct for this effect. Figure 9 shows the crossline component energy as a function of rotation angles for the 4-component waveform from shot 165 in Figure 8. It has been noticed that the energy minima of the two components are shifted by one degree. The two minima of E_{yx} are at $-67°$ and $23°$, respectively.

Results From the Linear Transform Method

The linear transform is first applied to the four component waveforms for shot 165. The results are presented in Figure 10. The time window was chosen with width 0.8 ms starting from 1.96ms. The waveforms shown are the principal time series obtained by this method. The angle α (in degrees) printed on the figure is the orientation of the upper source relative to the two principal anisotropy directions calculated with this technique. The angle $d\alpha$ printed on the figure is the orientation difference between the two sources due to the fact that they are at different depths. The td value is the time delay of the slow flexural wave. Changing the time window does not improve the results. This initial test demonstrates that the linear transform method gets acceptable results for this case. Figure 11 presents the two principal waveforms obtained by the linear transform for receiver number five. Figure 12 shows the strike direction α, the differences of azimuthal orientation between the two cross-dipole sources, and the travel time of the two principal flexural waves calculated from the 8 m section shown in Figure 7 (using six receivers) by this technique.

Results From the Non-Orthogonal Rotation Methods

Figures 13 to 15 show the results of applying non-orthogonal rotation to the same data set. The principal time series obtained are shown in the same way as in the Figures 10 to 12. These results are better than those obtained by the linear transform method.

Results From the Polar Energy Spectrum Technique

Figures 16 to 18 are the results from the polar energy spectrum method for the same data set. This technique is actually a method to find the principal directions by rotating the source and receiver separately. An additional advantage of this method is that it can tell if the sources are aligned with the receivers, and if there is any vertical variation of anisotropy within the formation between the source and receivers. The α_3 and α_4 values in Figure 18 show the source orientation relative to the principal directions determined by this technique. From the principal waveforms in Figure 17, it can be seen that there is an abrupt time shift at depth 3533.5 m. There is no direct way to check such an inconsistency. It is probably due to a miscalculation caused by interferences in the field measurements.

DISCUSSION

Because there is no absolutely objective way to check the results obtained by applying the three techniques to the ARCO dipole logs, only consistency and the variance of the data between all the receivers can be used to compare the techniques. It should be noted that the time window selection could have significant effects on the data processing results.

CONCLUSIONS

We have examined three methods for analyzing azimuthal anisotropy with cross dipole logging data from an anisotropic formation. These techniques, which were originally developed for VSP data processing, are based on the phenomena of flexural wave splitting in anisotropic materials. From the point of view of consistency and the standard deviation of the results from different source-receiver sets in the anisotropic section, the non-orthogonal rotation method works best. The linear transform technique also yields acceptable results, and has the advantage of using minimal computer time. The polar energy spectrum method is relatively sensitive to noise.

ACKNOWLEDGMENTS

We thank Dr. Keith Katahara of ARCO Oil and Gas Company for providing the data. We are grateful to Dr. Bertram Nolte for his tremendous help in preparing the logging data and providing related information. This research was supported by the Borehole Acoustics and Logging Consortium at ERL, the ERL/nCUBE Geophysical Center for Parallel Processing, and DOE Contract #DE-FG02-86ER13636.

REFERENCES

Alford, R.M., 1986. Shear Data in the Presence of Azimuthal Anisotropy. *56th S.E.G Annual Meeting Expanded Abstracts.* Houston, TX.

Barton, C. and Zoback, M., 1988. Determination of in situ stress orientation from borehole guided waves. *J. Geophys. Res., 93,* 7834-7844.

Ellefsen, K. J., 1990. Elastic wave propagation along a borehole in an anisotropic medium. Ph.D. Thesis, Massachusetts Institute of Technology, Cambridge, MA.

Esmersoy, C., Koster, K., Williams, M., Boyd, A. and Kane, M., 1994. Dipole shear anisotropy logging. *64th SEG Annual Meeting Expanded Abstracts.* Los Angeles.

Hatchell, P.J. and Cowles, C.S., 1992. Flexural borehole modes and measurement of shear-wave azimuthal anisotropy. *62nd S.E.G Annual Meeting Expanded Abstracts.* New Orleans, LA.

Igel, H. and Crampin, S., 1990. Extracting shear wave polarizations from different source orientations: Synthetic modelling. *J. Geophys. Res., 95,* 11283-11292.

Kanasewich, E.R., 1981. *Time Sequence Analysis in Geophysics.* University of Alberta Press. Third Edition.

Lefeuvre, F., Cliet, C. and Nicoletis, L., 1989. Shear-wave birefringence measurement and detection in the Paris Basin. *59th SEG Annual Meeting Expanded Abstracts.* Dallas, TX.

Li, X.Y. and Crampin, S., 1993. Linear-transform techniques for processing shear-wave anisotropy in four component seismic data. *Geophysics, 58,* 240-256.

Nolte, B. and Cheng, C.H., 1996. Estimation of non-orthogonal shear-wave polarizations and shear-wave velocities from four component dipole logs. M.I.T. Borehole Acoustic and Logging and Reservoir Delineation Consortia Annual Report.

Sinha, B. K., Norris, A. N. and Chang, S. K., 1991. Borehole flexural modes in anisotropic formations. *61st SEG Annual Meeting Expanded Abstracts.* Houston, TX.

Thomsen, L.A., 1988. Reflection seismology over azimuthal anisotropic media. *Geophysics, 53,* 304-313.

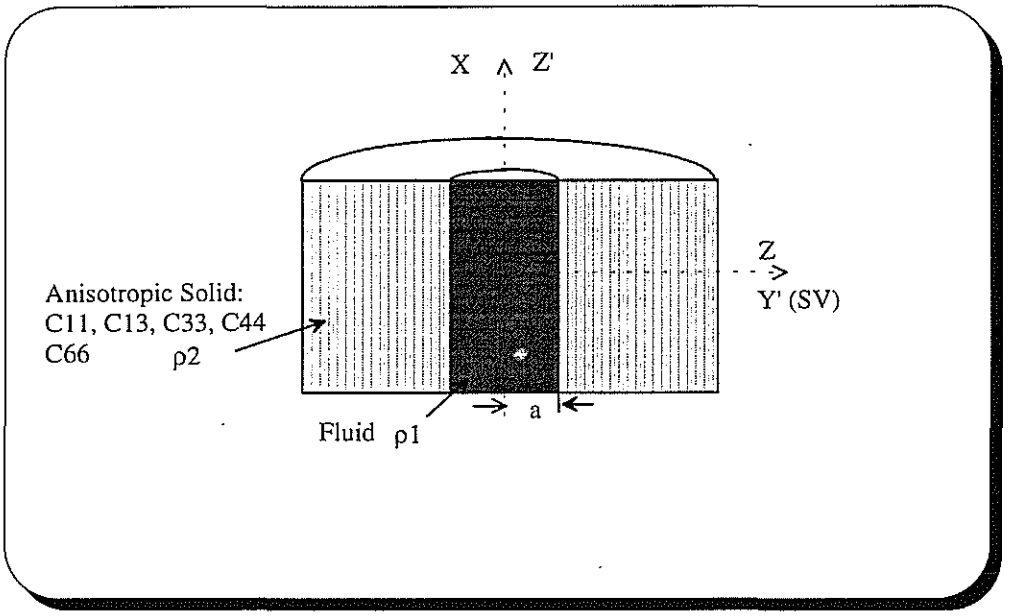

Figure 1: Schematic diagram of fluid-filled borehole of radius a. The surrounding formation exhibits the symmetry of a TI medium whose symmetry axis Z is normal to the borehole axis Z'.

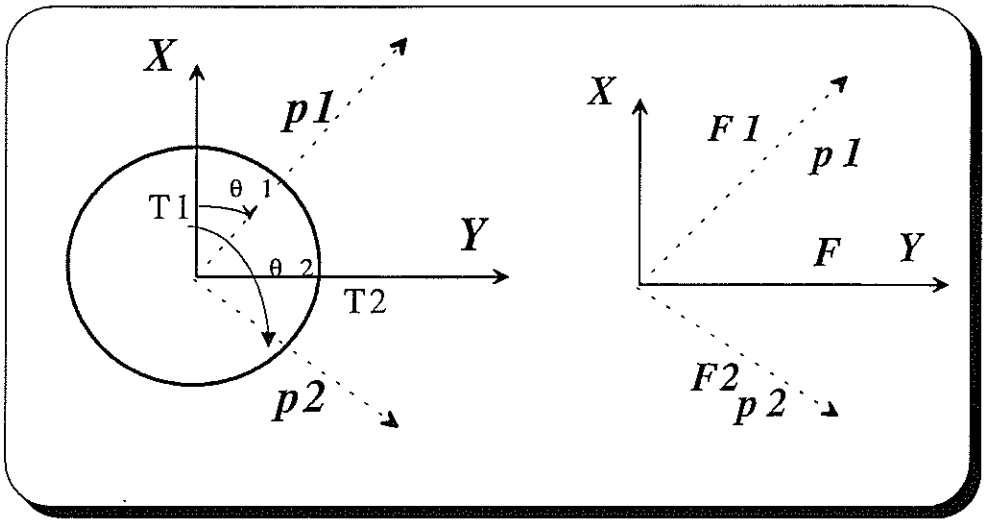

Figure 2: The coordinate system with origin at the transmitter or receiver plane. We assume that there is no angular misalignment between the transmitter and receiver section of the tool. Two orthogonal dipole transmitters, designated T_1 and T_2, are located at the same depth and on the axis of a vertical circular borehole. Two orthogonal dipole receivers,$R1$ and $R2$, are located on the axis of the borehole a distance L away from the transmitters.

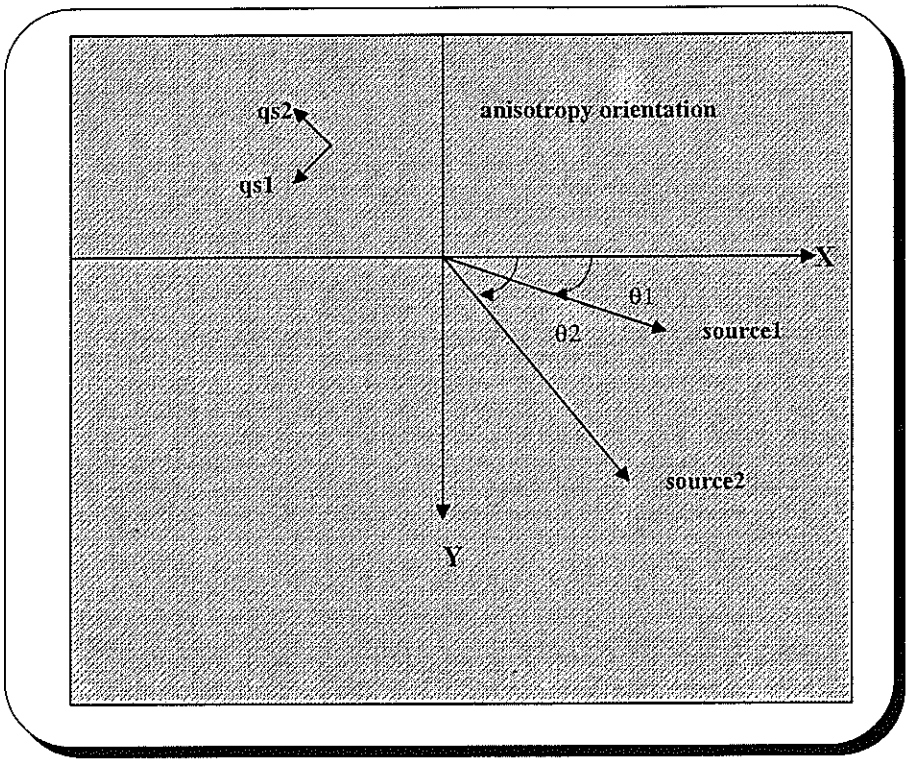

Figure 3: Coordinate system and azimuthal anisotropy directions in the polar energy spectrum model.

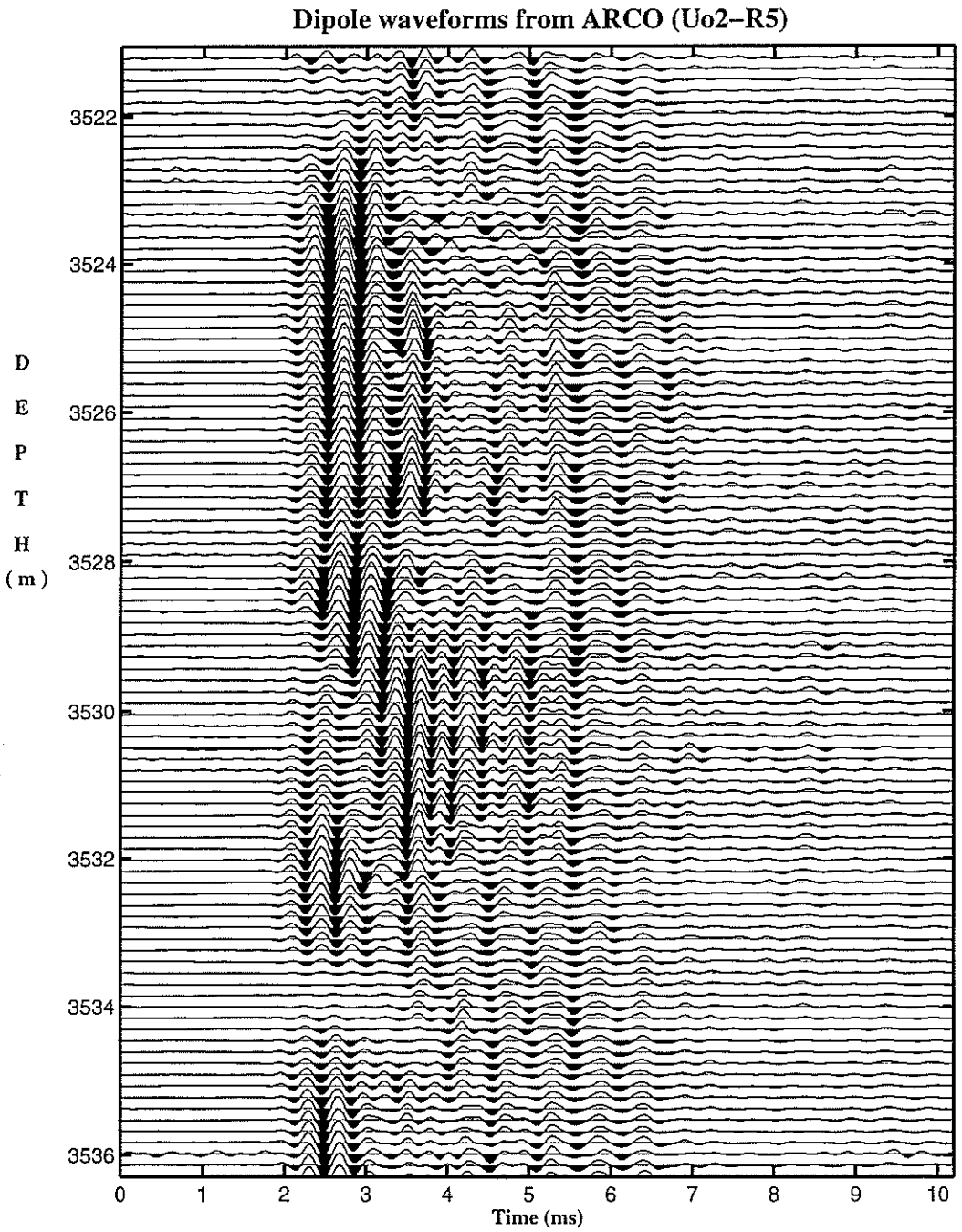

Figure 4: A section of the cross-dipole waveform (15.24 m or 50 ft from depth 3521 m to 3536 m), recorded from one cross-line measurement with the upper dipole source.

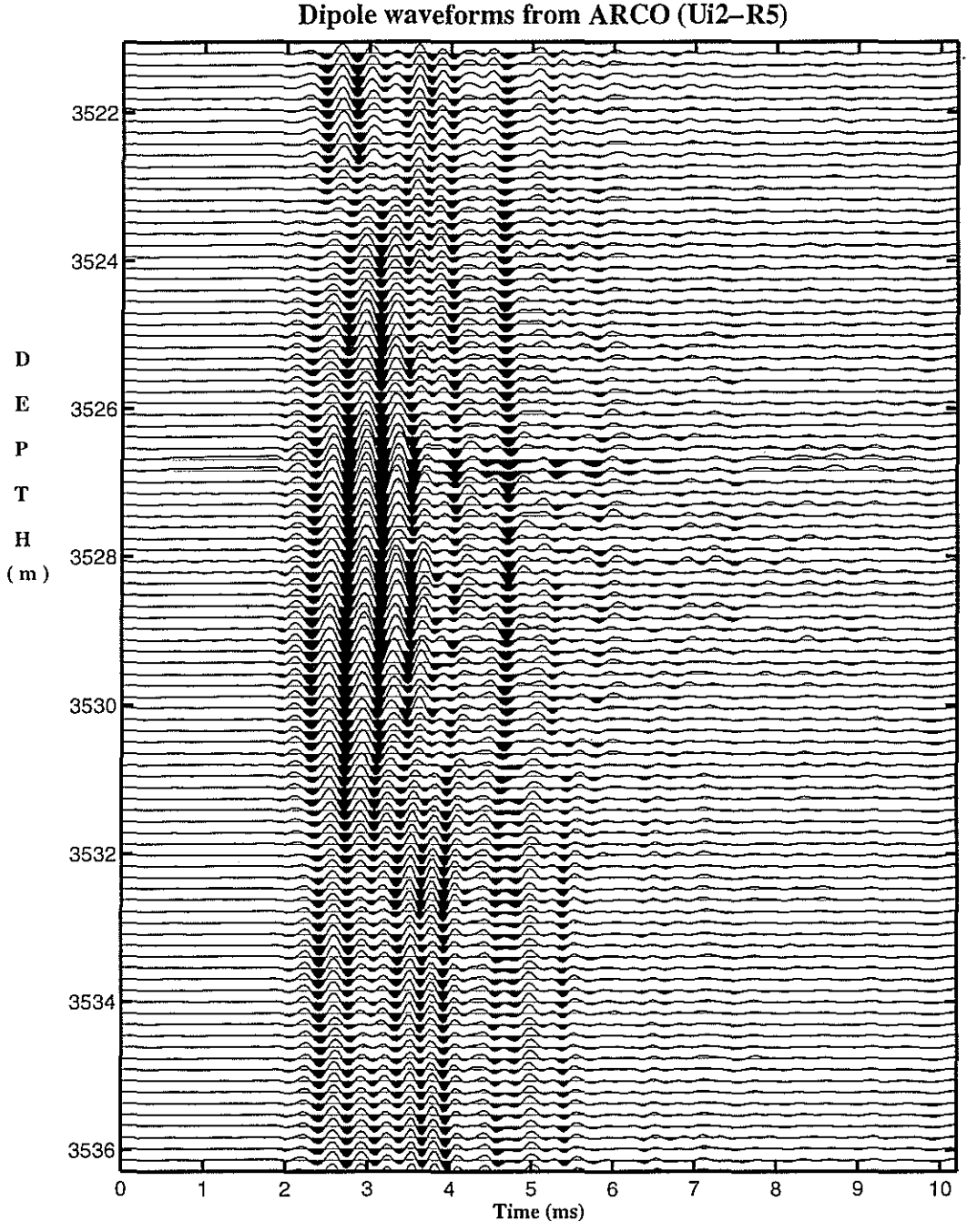

Figure 5: A section of the cross-dipole waveform (15.24 m or 50 ft from depth 3521 m to 3536 m), recorded from one in-line measurement with the upper dipole source.

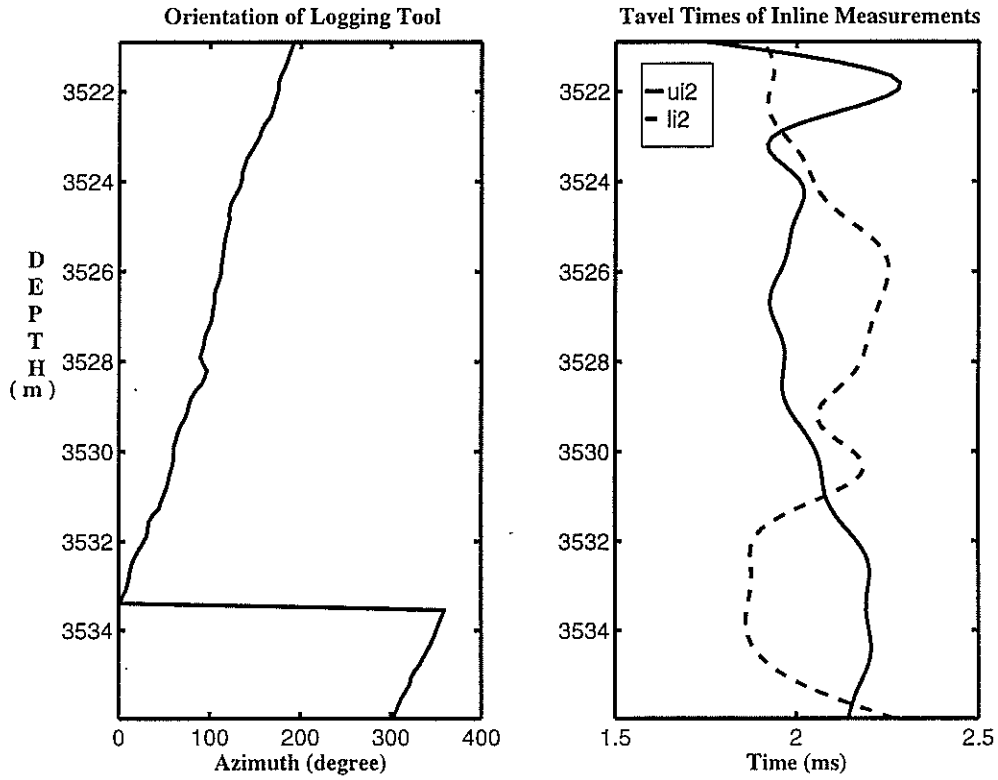

Figure 6: Dipole logging tool azimuthal orientation (left) recorded for the same section as in Figure 4, and the variation of travel times of the first (solid line) and second (dashed line) dipole in-line measurement at equal-offset receivers (right).

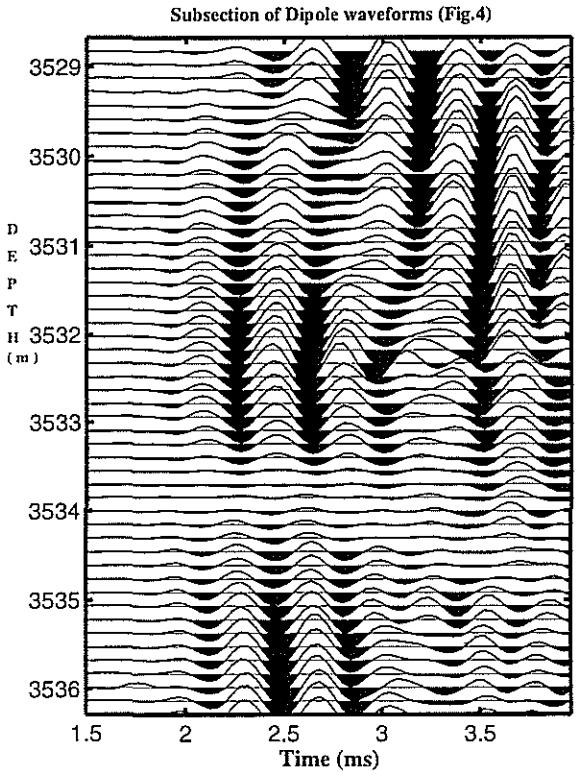

Figure 7: Cross component waveforms from an 8 m section in a time window from 1.5 ms to 4 ms.

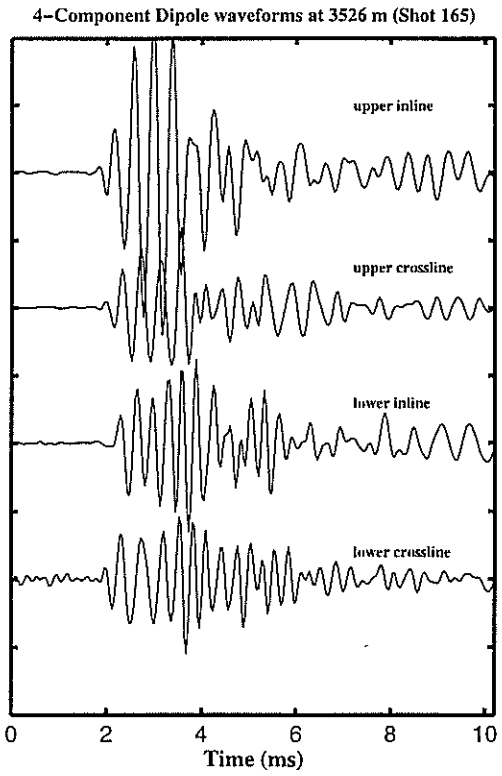

Figure 8: Four component waveforms from receiver number five at shot 165 taken from the section in Figure 7.

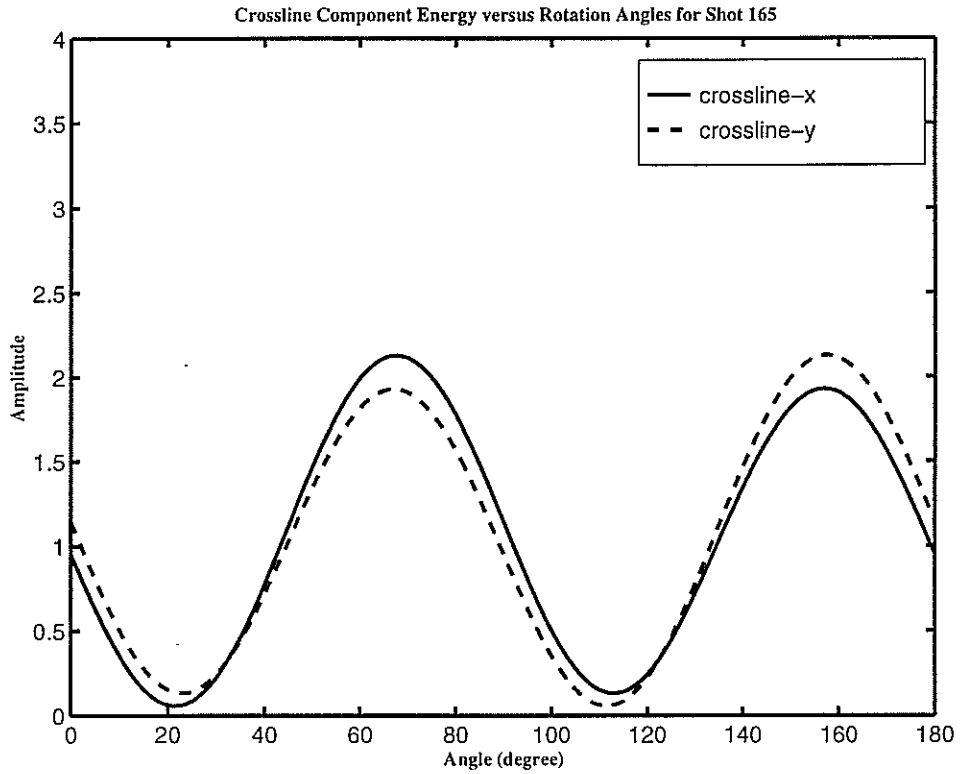

Figure 9: Crossline component energy as a function of rotation angles for the four component waveforms from shot 165 in Figure 8.

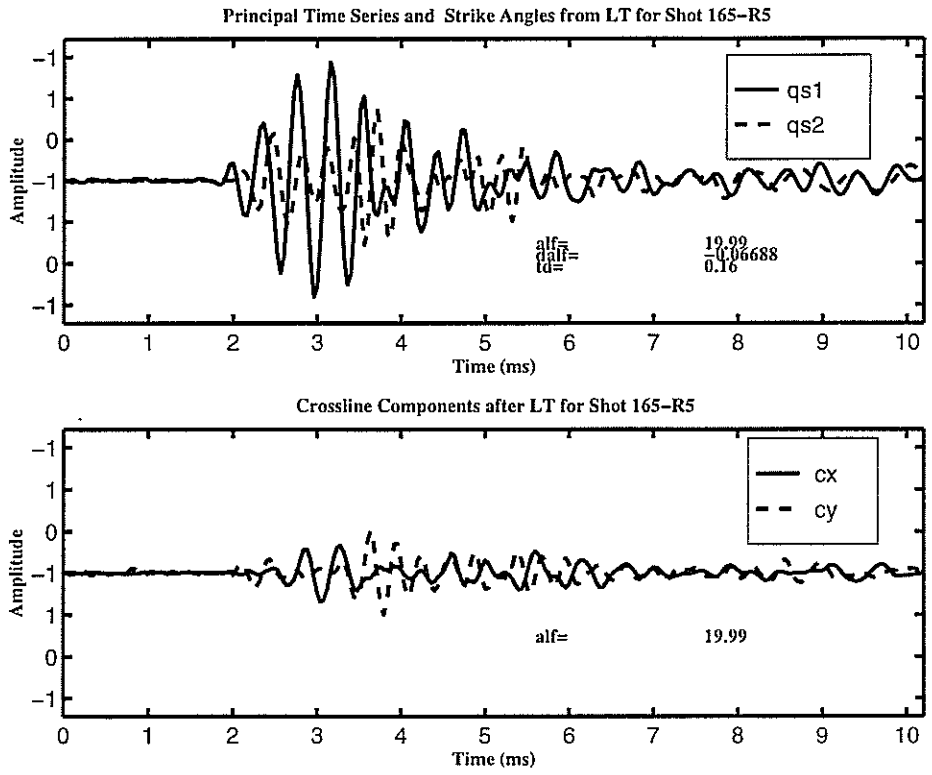

Figure 10: The results of applying the linear transform method to the four component waveforms of shot 165. An 0.8 ms time window was chosen starting from 1.96ms. The waveforms shown are the principal time series obtained. The angle α (in degrees) printed on the figure is the orientation of the upper source relative to the two principal anisotropy directions calculated with this technique.

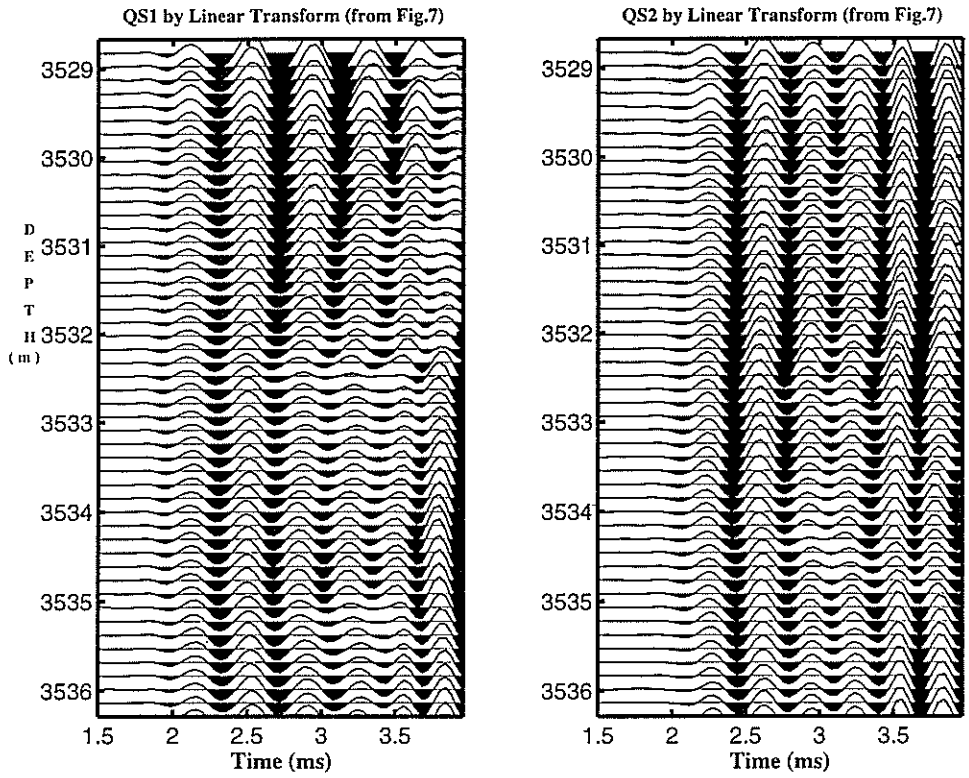

Figure 11: The two principal waveforms obtained by the linear transform method for receiver number five.

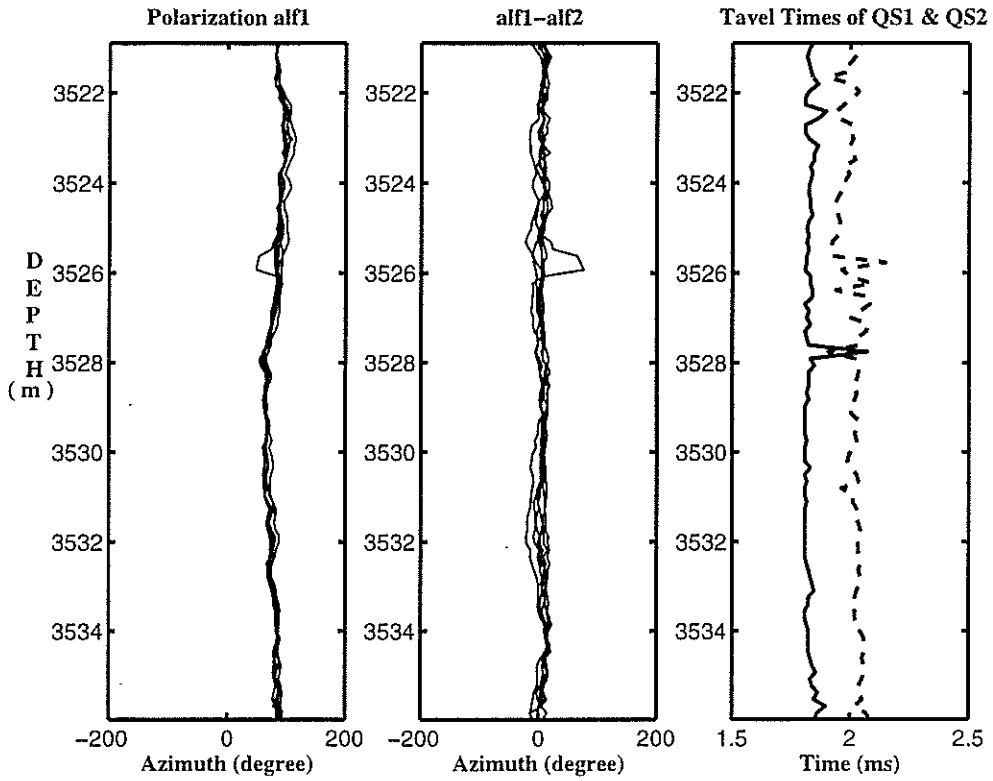

Figure 12: The principal direction α (left), differences of azimuthal orientation between the two cross dipole sources (middle) and the travel times of the two principal flexural waves calculated from the sub-data section in Figure 7 for 6 receivers by linear transform.

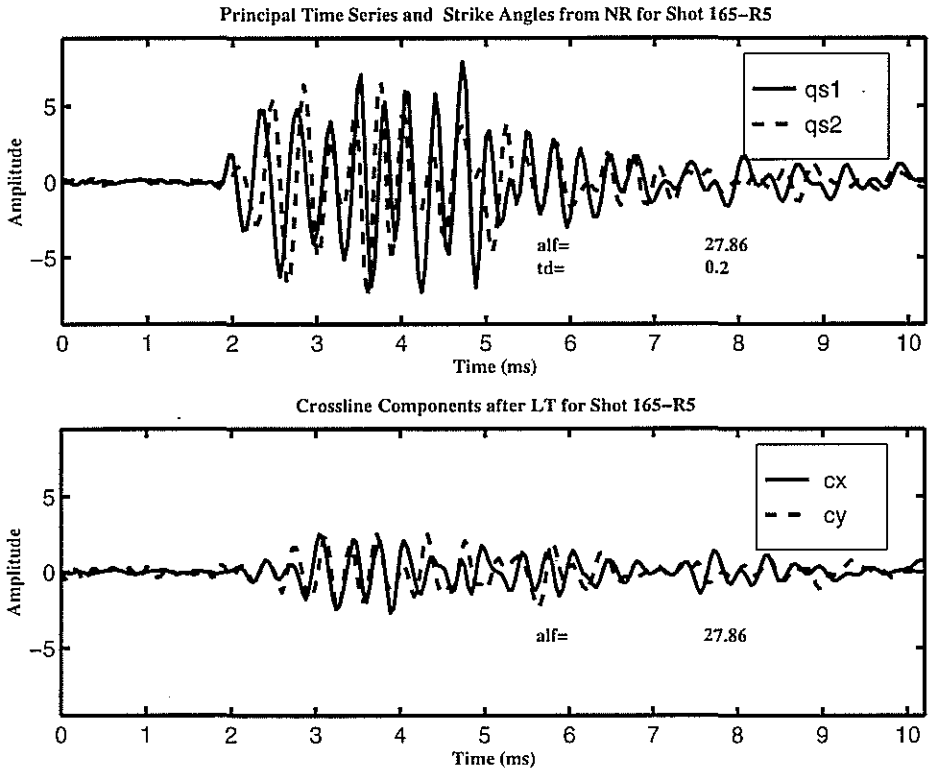

Figure 13: The results of applying the non-orthogonal rotation method to the four component waveforms of shot 165. An 0.8 ms time window was chosen starting from 1.96ms. The waveforms shown are the principal time series obtained. The angle α (in degrees) printed on the figure is the orientation of the upper source relative to the two principal anisotropy directions calculated with this technique.

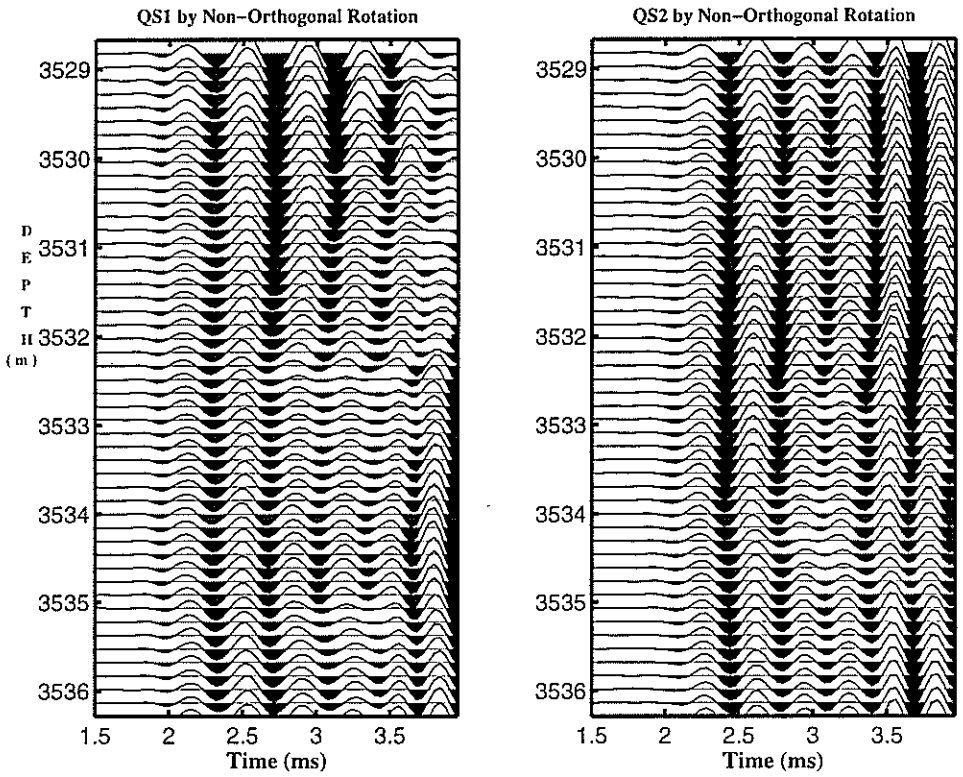

Figure 14: The two principal waveforms obtained by the non-orthogonal rotation method for receiver number five.

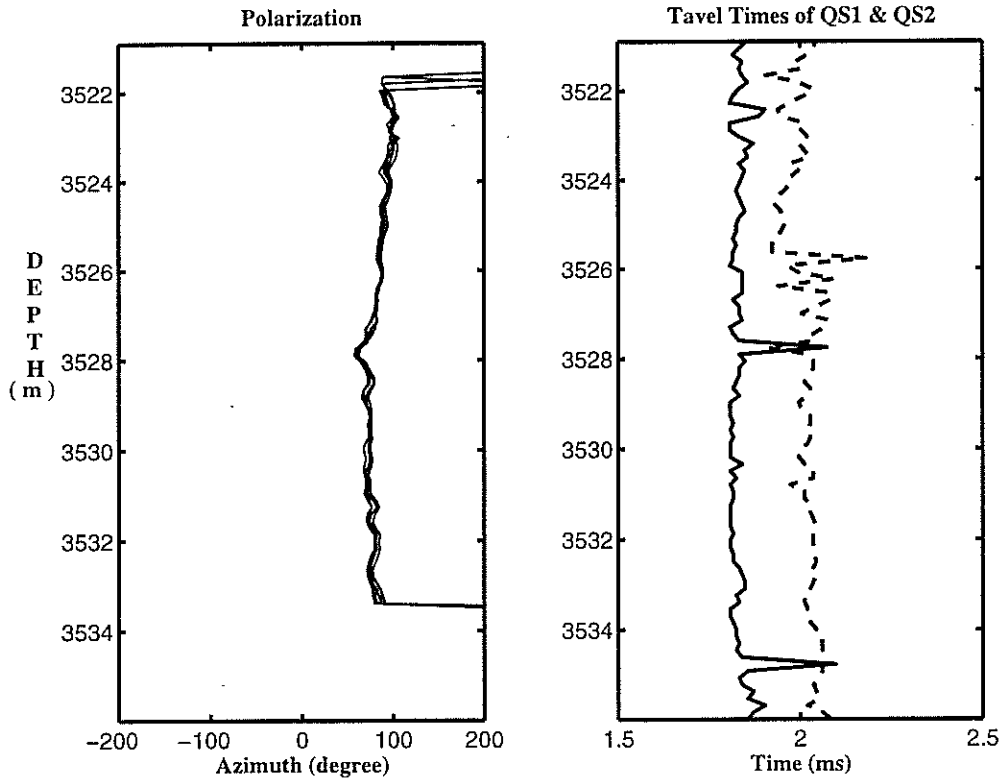

Figure 15: The principal direction α (left), the differences of azimuthal orientation between the two cross-dipole sources (middle), and the travel times of the two principal flexural waves calculated from the data in Figure 7 (using 6 receivers) by the non-orthogonal rotation method.

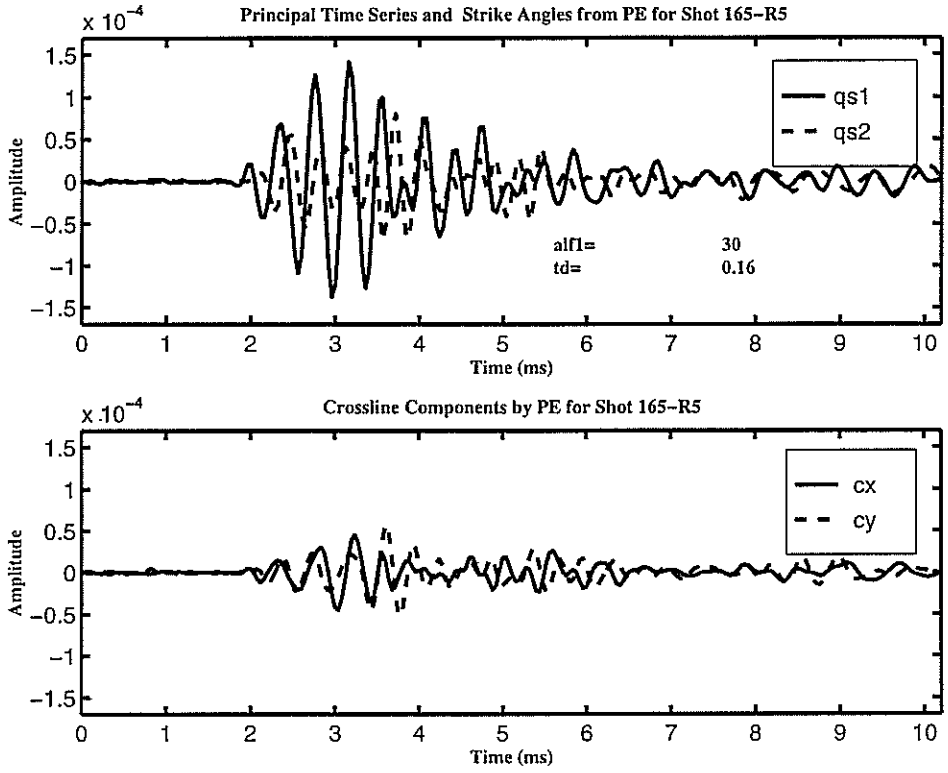

Figure 16: The results of applying the Polar Energy Spectrum method to the four component waveforms of shot 165. An 0.8 ms time window was chosen starting from 1.96ms. The waveforms shown are the principal time series obtained. The angle α (in degrees) printed on the figure is the orientation of the upper source relative to the two principal anisotropy directions calculated with this technique.

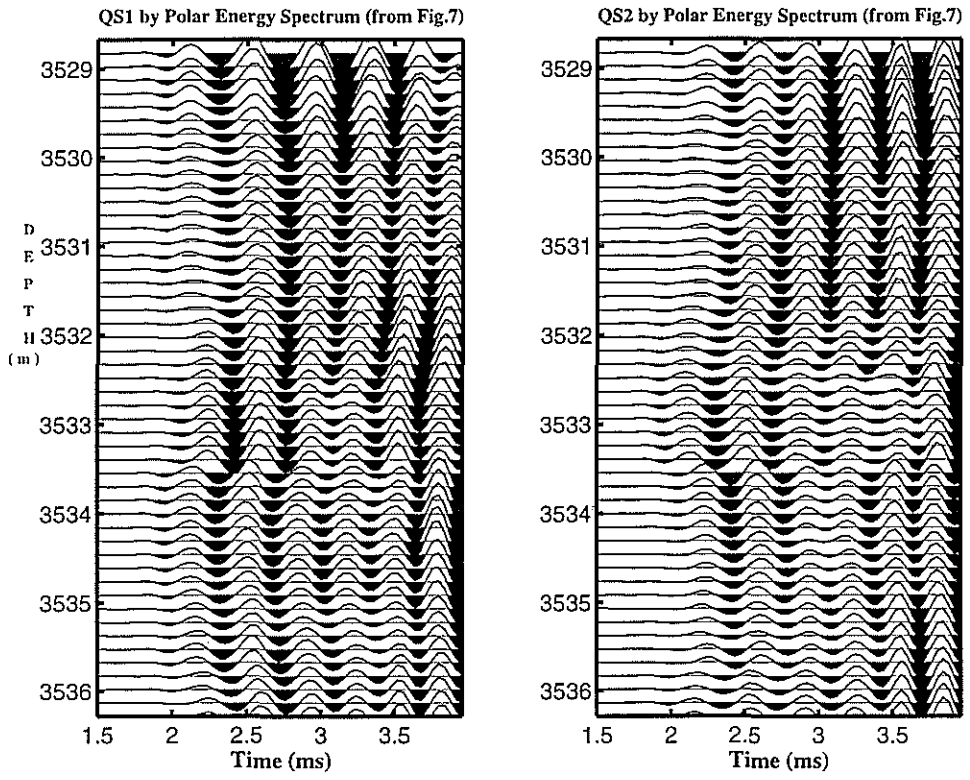

Figure 17: The two principal waveforms obtained by the Polar Energy Spectrum method for receiver number five.

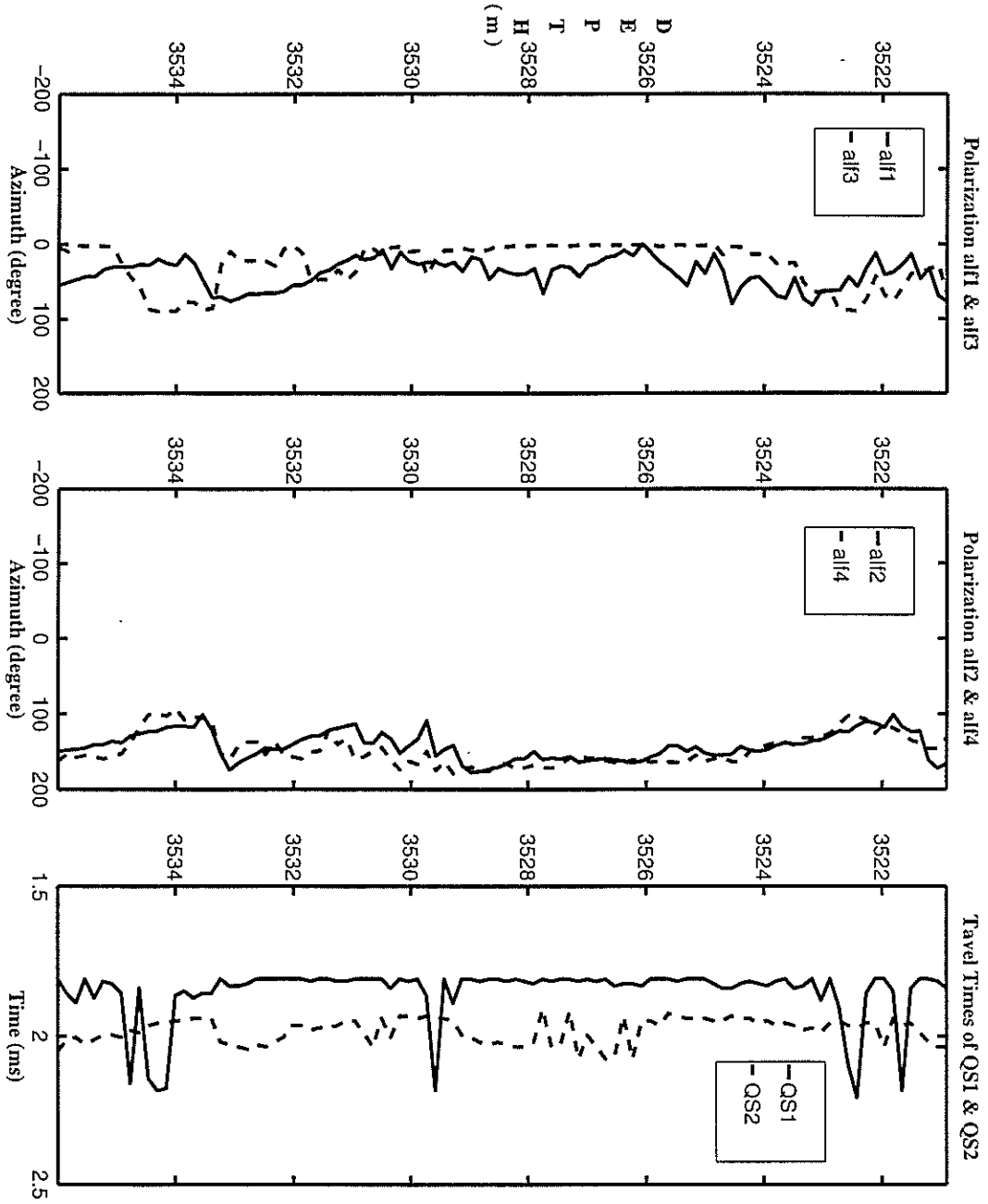

Figure 18: The principal direction α (left), differences of azimuthal orientation between the two cross-dipole sources (middle), and the travel times of the two principal flexural waves calculated from data in Figure 7 (using 6 receivers) by the Polar Energy Spectrum method.